DOE/MC/31178--5308
(DE97002048)

A Steerable/Distance Enhanced Penetrometer Delivery System Phase II

Topical Report

by
Ali Amini
Joram Shenhar
Kenneth D. Lum

May 1996

Work Performed Under Contract No.: DE-AR21-94MC31178

for

U.S. Department of Energy
Office of Environmental Management
Office of Technology Development
Washington, D.C.

U.S. Department of Energy
Office of Fossil Energy
Morgantown Energy Technology Center
Morgantown, West Virginia

by
UTD, Incorporated
Newington, Virginia

Disclaimer

DOE/MC/31178--5308
(DE97002048)

A Steerable/Distance Enhanced Penetrometer Delivery System Phase II

Topical Report

by
Ali Amini
Joram Shenhar
Kenneth D. Lum

May 1996

Work Performed Under Contract No.: DE-AR21-94MC31178

for

U.S. Department of Energy
Office of Environmental Management
Office of Technology Development
1000 Independence Avenue
Washington, D.C. 20585

U.S. Department of Energy
Office of Fossil Energy
Morgantown Energy Technology Center
P.O. Box 880
Morgantown, West Virginia 26507-0880

by
UTD, Incorporated
8560 Cinderbed Road
Suite 1300
Newington, Virginia 22122

TABLE OF CONTENTS

LIST OF FIGURES

Page

LIST OF FIGURES (con't.)

Page

EXECUTIVE SUMMARY

Penetrometers play an important role in detection, mapping and remediation of underground contaminated sites. At present, penetrometer applications are restricted mainly to vertical pushes. This is due to a technology gap that exists in tracking and steering of the penetrometer tip. In the past five years, UTD Incorporated has worked to close this technology gap by developing an accurate and efficient position location system referred to as the POLO (POsition LOcation) device.

The prototype POLO device was developed under a PRDA contract sponsored by the Department Of Energy (DOE), Morgantown Energy Technology Center (METC), Office of Science and Technology. At the completion of this contract, for the first time the penetrometer operator had the capability to know the position of the tip of the penetrometer in real- time. Building on this capability, UTD Incorporated was awarded a follow-on three-phase contract under a Research Opportunity Announcement (ROA) program. The objectives of the new contract are to develop a steerable distance enhanced penetrometer delivery system, and to integrate POLO into a commercial penetrometer truck.

The Phase I work was the base year program and was comprised of sub-scale (smaller scale for the purpose of laboratory testing) major sub-systems analysis and design of steering and vibratory penetrometer components. In addition, the Phase I work was modified to include the integration of a POLO system into a commercial penetrometer truck. Through the analysis, design work and laboratory and field tests carried out in Phase I, the feasibility of a steerable penetrometer delivery system was demonstrated. In addition, it was shown that vibratory penetration increases depth of penetration by reducing the magnitude of the retarding forces on penetrometer rods.

The work in Phase II summarized in this report was carried out to generate an integrated design of a full-scale steerable/distance enhanced penetrometer delivery system. Three main tasks were completed, including systems analysis (Task 2.1), steerable system component integration (Task 2.2), and integrated design of the vibratory penetrometer system (Task 2.3). Under Task 2.1, the operational envelopes for all the sub-systems were defined. The sub-systems analyzed included the steering system (steering tip, steerable locking joints, and a steering torque mechanism), the vibratory/thrusting system, the POLO navigational system, and an anchoring system for the penetrometer rig.

Under Task 2.2, the components of the steerable system were analyzed and redesigned when necessary for integration into the overall full-scale penetrometer system. The results of this task include design drawings and specifications for the steering tip, steerable locking joints, and a steering torque mechanism.

Under Task 2.3, the vibratory/thrusting system, the POLO system and the anchoring mechanism were analyzed and redesigned when necessary for integration into the overall full-scale penetrometer system. The results of this task include design drawings and specifications.

The results of Phase II work will be used to manufacture and assemble a full-scale system for field trials and demonstrations in Phase III.

1.0 INTRODUCTION

1.1 Background

The characterization, monitoring, and remediation of many of the nation's highly contaminated sites are among the highest priorities of the Department Of Energy (DOE). In underground contaminated sites, detection and mapping of the plume of contamination and in-situ remediation are the first steps towards clean up. The needs for these steps include a depth capability ranging from tens of feet to between 100 to 200 feet, ability to go around underground obstacles with curvatures that do not damage downhole components, and downhole access for delivery of environmental sensors. In addition, in some instances it is necessary to use lightweight equipment over underground storage tanks. Baseline technologies of "aim and shoot" well drilling do not satisfy all of these needs, are not as efficient, and can further contaminate the site by bringing underground contaminants to the surface. As a result, new technologies are needed to carry out underground site clean up more efficiently.

One system which has provided significant efficiency over baseline well drilling technology is the penetrometer. Using penetrometers, rods with an instrumented tip are pushed into the ground incrementally. In traditional penetrometer applications, the instrumentation package located at the tip measures soil resistance. However, for environmental monitoring purposes, an array of environmental sensors are packed inside the penetrometer rods for in-situ sampling and analysis, or for retrieval of laboratory samples. Examples of these sensors include soil samplers, the BAT groundwater monitoring sampling system, the PRT system for vapor sampling and the LIF system for in-situ detection of contaminants.

At present, penetrometer applications are restricted primarily to vertical pushes on the order of 100 to 200 feet. Because of their heavy weight, the use of penetrometer trucks over shallow buried storage tanks is restricted and costly. To close the technology gap in the use of penetrometers for environmental purposes, UTD took the first step by developing a new position location device for penetrometers referred to as POLO (short for POsition LOcator), which provides real-time position location without blocking downhole access for environmental sensors. The next step taken was the initiation of work to make penetrometers steerable and capable of greater penetration capabilities. The product of this work will be a relatively lightweight steerable penetrometer that can provide greater penetration capability than traditional penetrometers of the same weight.

Competitive technologies for POLO include tilt sensors placed at the tip of penetrometers, accelerometers and magnetometers. Tilt sensors can only provide the tilt angle of the tip without providing information for real time tracking of the tip in three dimensions. Accelerometer arrangements that can provide data for real time tracking are expensive and block access to the tip of the penetrometer. Magnetometers are expensive and their capability is affected by magnetic anomalies.

A competitive technology for steerable penetrometer is directional drilling. Directional drills are used mostly for installation of underground pipes and utility cables. They use large

amounts of water for drilling purposes and bring the cuttings to the surface. The problems with this technology are that the water used for drilling can spread the contamination further into the ground and the cuttings brought to the surface have to go through a clean up process.

The initial development of POLO was carried out through internal funds at UTD. Realizing the benefits of this new technology, DOE Morgantown Energy Technology Center (METC) funded the development of a prototype system under a PRDA contract. At the completion of the PRDA contract in September, 1994, for the first time the penetrometer operator had the capability to know the position of his sampling locations. Building upon this capability, DOE awarded UTD a new contract to develop a steerable distance enhanced penetrometer delivery system. The new contract was awarded under a Research Opportunity Announcement (ROA) program and is comprised of a base program (Phase I) and two optional phases (Phases II and III).

Phase I of the contract was completed in August of 1995 (Reference [1]). This report presents the results of the second phase of the contract.

1.2 Objectives

The overall objectives of the contract are to complete the development of a steering capability, and a vibratory thrusting capability for penetrometer delivery systems. Steering provides the means for controlled and directional use of the penetrometer, and vibratory thrusting can provide greater penetration capability. To achieve these objectives, the overall effort was divided into three phases.

The objectives of Phase I included analysis, design, and laboratory testing of the individual sub-systems required to perform vibratory thrusting and steering of penetrometers. These objectives were accomplished, demonstrated and summarized in Phase I final report [1].

The main objective of Phase II was full-scale system design integration. To achieve this objective, the design of all the sub-systems that were developed and tested in Phase I were examined and modified as necessary in order to be integrated into a full-scale, field deployable system. The sub-systems included the steering tip, POLO, steerable rod joints, torque mechanism, and the vibratory/thrusting rig.

The objectives of Phase III will be to manufacture full-scale components and to demonstrate the full-scale integrated system in a series of field tests.

1.3 Scope of Work

The tasks completed in Phase I included prototype steerable tip analysis, manufacturing and testing; acquisition of a META-DRILL unit (vibratory rig); design, manufacturing and testing of rod joints suitable for steering; theoretical systems analysis; and laboratory and field testing of individual components. In addition, through an in-scope modification of the contract a commercial POLO system was integrated into DOE's SCAPS penetrometer truck.

The tasks of Phase II include:

Full-Scale System Design Integration

Task 2.1 Systems Analysis

Operational envelopes for all the sub-systems were defined. The sub-systems analyzed included the steering system (steering tip, steerable locking joints, and a steering torque mechanism), the vibratory/thrusting system, the POLO navigational system, and an anchoring system for the penetrometer rig.

Task 2.2 Steerable System Component Integration

The components of the steerable system were analyzed and redesigned when necessary for integration into the overall full-scale penetrometer system. The results of this task include design drawings and specifications for the steering tip, steerable locking joints, and a steering torque mechanism.

Task 2.3 Vibratory Penetrometer System Integration

The vibratory/thrusting system, the POLO system, and the anchoring mechanism were analyzed and redesigned when necessary for integration into the overall full-scale penetrometer system. The results of this task include design drawings and specifications.

Detail findings of tasks 2.1 through 2.3 are presented in subsequent sections of this report.

2.0 SYSTEMS ANALYSIS

The overall penetrometer system being demonstrated under this contract is made up of the following sub-systems:

- Steering system which includes a steering tip, steerable locking joints and a steering torque mechanism.
- Vibratory/Thrusting system which includes the META-DRILL and its hydraulic control sub-systems.
- POLO system which includes a POLO rod, downhole electronics, quick connects, an initializer and a computer.
- Anchoring system which includes screw anchors and anchor blocks.

Under the Systems Analysis task (Task 2.1), operational envelopes for all the sub-systems were defined. Operational envelopes for the steering system included charts showing the lateral reach of the steering tip (penetrometer rod trajectory), and the expected radius of curvature of the penetrometer rods. In addition, the forces (and the resulting stresses) necessary to push penetrometer rods to a certain depth were calculated. The envelopes were calculated by modeling the penetrometer rods as a series of beams subjected to resisting loads at the tip of the penetrometer and frictional resistance along the outer surface of the rods.

The envelopes for the vibratory/thrusting systems included hydraulic and vibratory force limits of the META-DRILL rig. This is the rig that will serve as the main platform for the steerable vibratory penetrometer delivery system. The envelopes were defined based on manufacturer data and field testing of the META-DRILL.

Operational envelopes for the POLO system included the force and strain limits of the downhole POLO rod. These envelopes were calculated based on design drawings of the rod. The envelopes for the anchoring system of the META-DRILL included pull-out force limits under vibratory loading conditions. They were calculated based on field tests and specifications for the META-DRILL.

Before presenting the operational envelopes, it will be useful to review the sub-systems.

Steering System

The steering system of the penetrometer includes a steering tip, steerable joints, and a steering torque mechanism. Several design options were considered in Phase I, some of which were of the passive tip configuration while others were associated with active tip mechanisms. All options considered for transverse force generation involved tips formed as a simple wedge or an oblique cone.

Using the passive tip approach, a fixed tip configuration is installed. Pushing of the penetrometer rod with such a tip generates rod deflection constantly. In order to reach a specified

target, on-line tip position detection coupled with continuous reorientation of its transverse bending force is essential. Obviously, these activities must be commanded from the ground surface that calls for the application of an increasing continuous axial torque to the entire penetrometer rod system. In long pushes the constant reorientation of the tip from the surface can slow down the penetration process considerably.

The active tip approach involves a mechanical tip installed at the rod front end that can be actuated to turn or change its position through signals sent from the surface. A tip for this purpose will have many mechanical parts and will require an umbilical for the actuation signals. Because of the vibratory nature of the penetration process, a mechanical tip with many parts is susceptible to breakdown and fatigue failure of components and connections. In addition, the actuation signal umbilical occupies a fairly large volume inside the penetrometer rods, leaving little or no space for the umbilical of the environmental sensing instruments.

Realizing the disadvantages of the fully passive or fully active steering tips, it was decided to use a semi-passive tip developed by Foster-Miller Incorporated for ground piercing applications. The advantages of the semi-passive tip are that the tip does not have to be reoriented continually from the surface, and it is made with very few mechanical parts, making it easy to use and control in the field. If an unexpected barrier is encountered the penetrometer tip can be drawn back and redirected to maneuver around the barrier.

The steering tip is shown in Figure 1. The tip has two modes of operation. In the configuration shown to the left of Figure 1, the tip is in its straight pushing mode, whereas in the configuration to the right, the tip is in its steering position. The switch between the two modes is accomplished by a 180 degree turn of the rod portion of the tip. Once the switch to a steerable mode is accomplished the now-asymmetric tip must be brought to the desired toolface angle. This is done by continuing the tool rotation in the same direction. As the rod is turned, the fins on the conical section of the tip keep the cone from turning in the soil. The fins play two other important roles in keeping each mode of operation of the steering tip stable. First, the fins are bevel biased so that in the symmetrical cone configuration, a clockwise torque is generated on the cone which keeps the cone rotated against its symmetrical position stop [2]. Second, one of the fins has a slightly larger area than the other which causes a counter-clockwise torque to be generated during pushing in asymmetrical configuration. This torque will keep the cone rotated against its asymmetrical position stop.

A prototype of the steering tip was manufactured and tested successfully in Phase I. During these tests the cone was pushed in a straight configuration under vibratory loading to a certain depth at which a counter-clockwise torque was applied to penetrometer rods from the surface. After this point continued pushing resulted in a curved path. At the completion of the test and upon retrieval of the cone it was visually verified that the cone tip had turned to its asymmetrical mode.

In traditional penetrometer applications rods are pushed vertically into the ground. However, in a steerable penetrometer, in order to reach the target of interest the rods are pushed into a curved path. In addition to bending due to a curved path, in order to change the mode of operation of the

steering tip, penetrometer rods will be subjected to steering torques. In Phase I it was shown that off the shelf penetrometer rods failed at relatively shallow curvatures (85-100 ft radius of curvature). As a result, a UTD steerable joint concept was adapted to be used with the steerable penetrometer. In addition, in order to prevent the rod joints from opening under the steering torque, a locking mechanism was designed for the steerable joint.

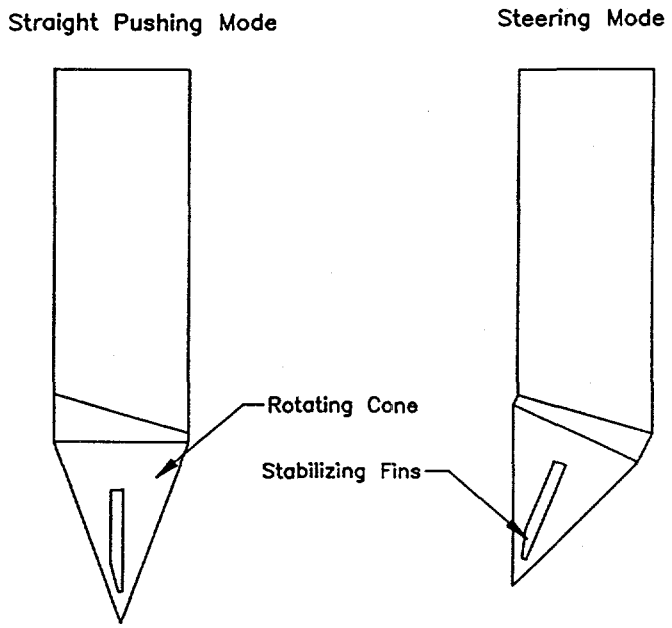

Figure 1. Modes of operation of the steering tip.

Figure 2 shows the components of the locking joint tested in Phase I. In order to assemble the joint it is necessary to thread the male and the female parts until the female fingers are aligned with the male splines. Then the shear plate ring is moved forward (moved from right to left in Figure 2) until it locks the male splines to the female fingers. Figure 3 shows the assembled locking joint. Although in Phase I the performance of the steerable locking joint of Figure 2 was demonstrated to be satisfactory, the assembly of the joint in the field was deemed to be cumbersome. Therefore, in Phase II the steerable joint design was refined for easier assembly in the field. Laboratory tests on the redesigned joint showed that it performs similarly to the joints tested in Phase I, but has the advantage of being easier to assemble in the field and more economical to manufacture.

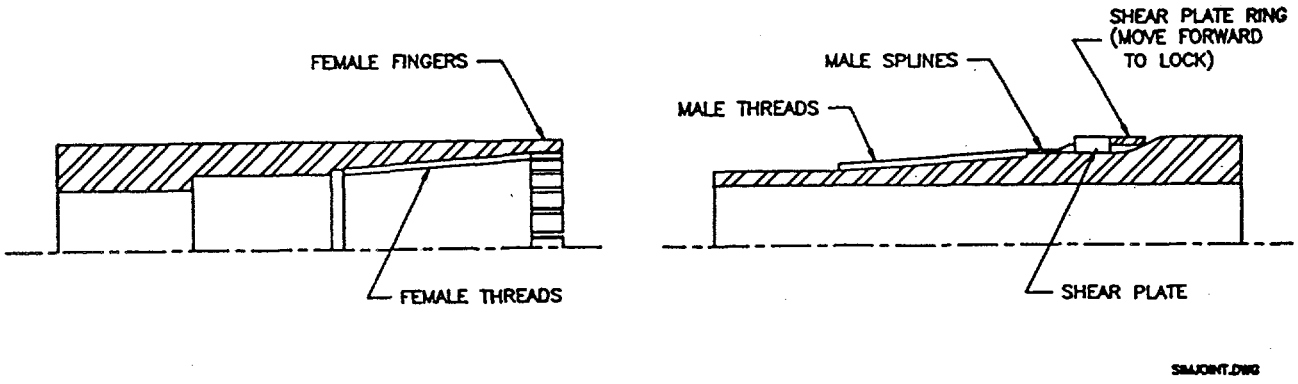

Figure 2. Steerable and locking rod joint designed in Phase I.

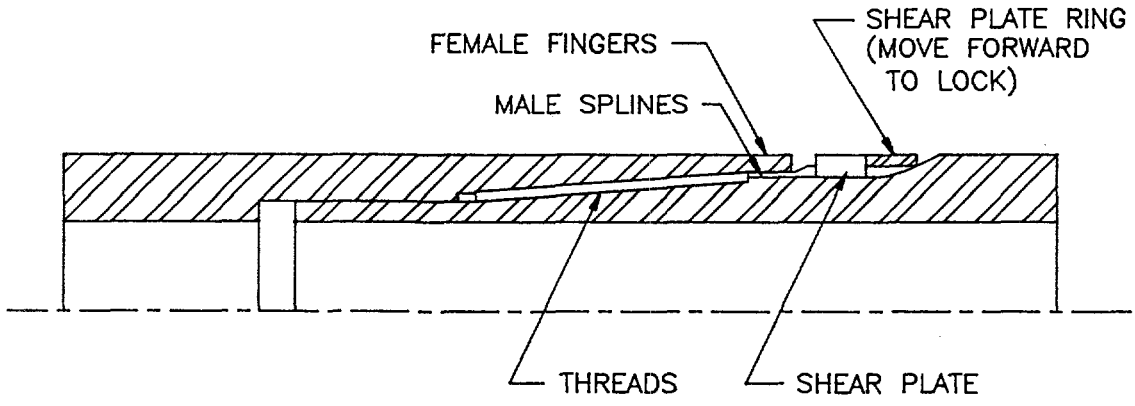

Figure 3. Assembled steerable and locking rod joint.

A steering torque mechanism is needed to tighten the steerable joints, and to apply the necessary torque for turning of the steering tip. This mechanism was designed on a preliminary basis in Phase I. Under task 2.2, in addition to integrated design of steerable rod joints, the preliminary design of the torque mechanism was finalized for integration into the overall system. The integrated design discussed in detail in Section 3.3 incorporates a hydraulic cylinder and two pipe wrenches for application of steering torques.

META-DRILL

During the Phase I contract a search was performed to select and purchase an appropriate penetrometer delivery system. The systems considered included commercial sonic drilling rigs, commercial vibratory penetrometer trucks, and vibratory coring equipment. To enable an appropriate selection, the information related to operating envelopes, reliability, user friendliness, and adaptability were compared with the requirements of the system.

The selected vibratory system is called META-DRILL (shown in Figure 4) and is manufactured by MPI Drilling. An important feature of the META-DRILL is its modular construction. The system is made up of five modules that can be upgraded or replaced separately. These modules include the META-PRESS (mast module), vibratory drive, control module, hydraulic reservoir module, and power module.

The META-DRILL was used successfully in field tests of Phase I. Under task 2.3 the necessary design work was carried out to integrate the rig with the rest of the steerable penetrometer system. This included design integration of POLO and an anchoring mechanism for the META-DRILL trailer. A detail discussion of Task 2.3 results are presented in Section 4.

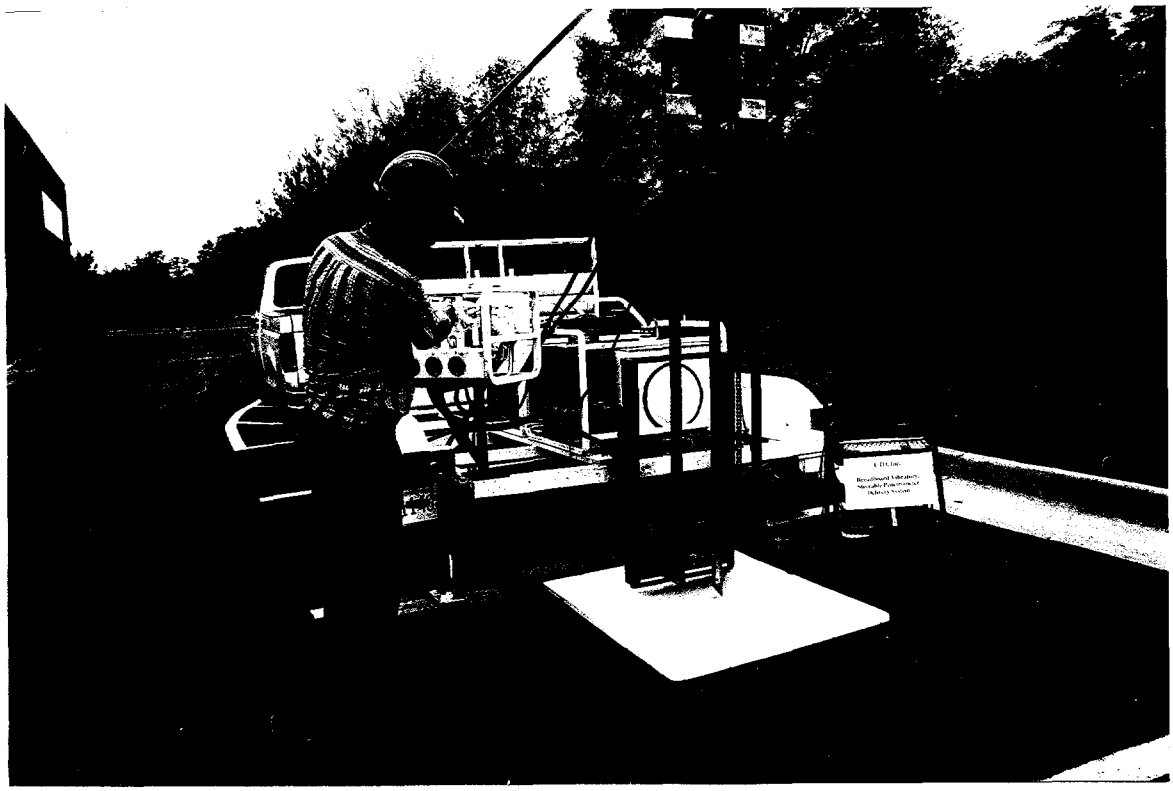

Figure 4. META-DRILL vibratory Penetrometer system.

POLO

POLO is the navigational unit of the overall system. It is a patented system that was developed under the sponsorship of the DOE METC, Office of Science and Technology. The POLO system has four main modules as shown in Figure 5. They are the POLO rod module, the data acquisition module, the POLO initilizer and the data processing module (computer).

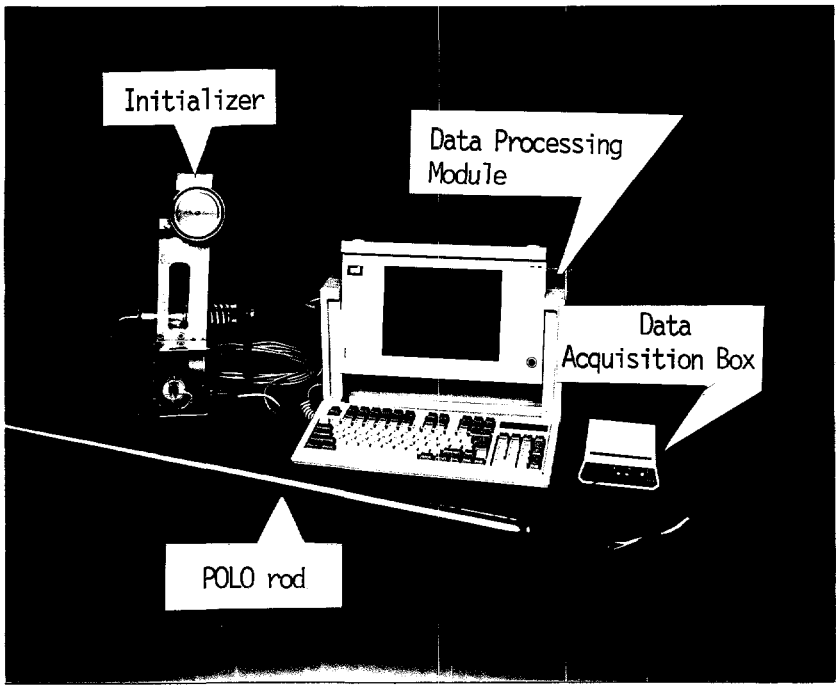

Figure 5. The POLO system.

The POLO rod module is the sensing element of the system. It is strain gaged in a way that enables the bending strains of the module to be measured as the POLO rod is pushed into the ground. The strain signals are processed by a downhole data acquisition microprocessor and sent to an uphole processor box via a two conductor umbilical. The uphole processor box is linked to a portable personal computer which runs the POLO tracking program.

The POLO tracking program converts strain readings of the POLO rod to global coordinates of the penetrometer at the end of each shove. To start tracking, initial angles of the POLO rod just before it is pushed into the ground are needed by the tracking program. The POLO initializer is used for this purpose.

There are three angles that completely describe the global orientation of the POLO rod: the elevation, azimuth and rotation angles as shown in Figure 6. The elevation angle is the angle between the horizon and the longitudinal axis of the POLO rod. The azimuth angle is the angle between a vertical plane which includes POLO and a northerly line. The rotation angle describes the orientation of the reference strain gage with respect to the plane containing the elevation angle.

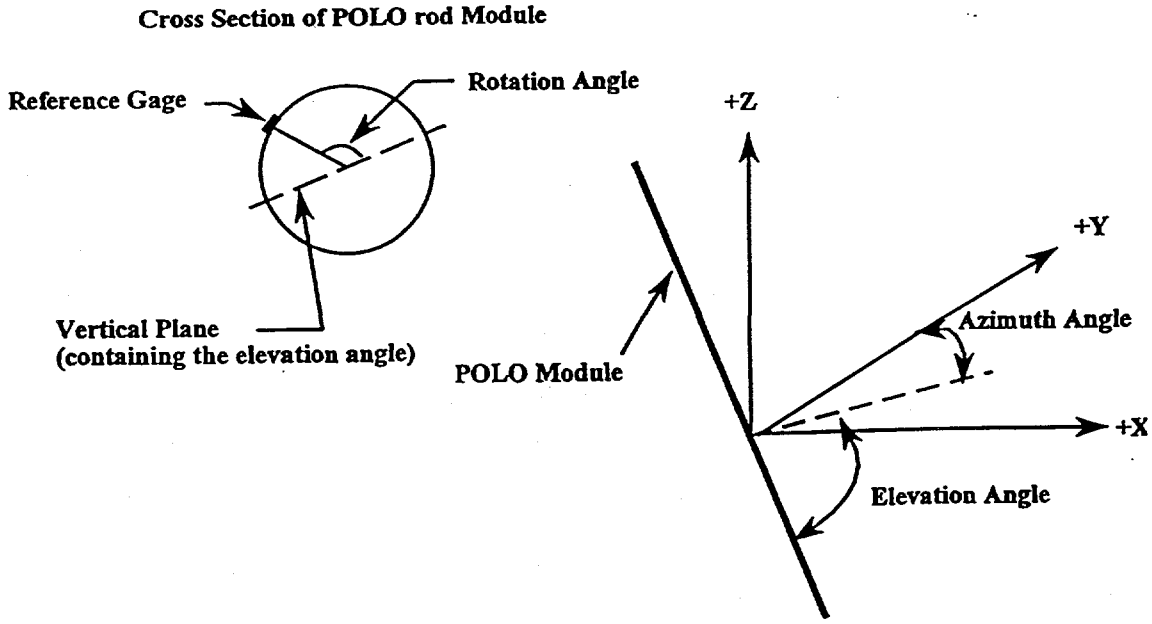

Figure 6. Initial angles of POLO.

When the initializer is attached to the POLO module, the two initializer clinometers read the elevation angles of two orthogonal axes perpendicular to the longitudinal axis of POLO. Using these two angles and trigonometric relations, the elevation, and azimuth angles of POLO are calculated by the POLO program.

In addition to providing the elevation and azimuth angles, the initializer can be used to load the POLO module along a predetermined bend plane by turning the hand wheel on the initializer. Once the POLO module is loaded, the POLO program automatically calculates the location of the reference gage on the module body with respect to the predetermined bend plane and calculates the rotation angle accordingly.

As shown in Figure 7, the initilizer is attached to the POLO rod module under the penetrometer truck. After the initialization is completed, the initilizer is removed and the normal penetration process begins.

In Phase II, the design of the POLO system was integrated with the overall penetrometer system. The main component of this integration is a connector called Quick-Connect which eliminates the use of a continuous POLO umbilical from downhole to the surface computer. The concept is explained in more detail in Section 4.1.

Figure 7. POLO initialization in progress.

Anchoring System

META-DRILL can provide up to 6,000 lbs of thrust on penetrometer rods. However, the rig itself is lightweight and can only provide approximately 1,500 lbs of reaction force before it lifts off the ground. Therefore, in order to apply the full 6,000 lbs of thrust, the rig has to be anchored to the ground. In Phase II, a preliminary screw anchoring system was tested in the field. Based on these test results the system was modified and its design was integrated with the design of the overall penetrometer system. The concept is explained in more detail in Section 4.2.

2.1 Operational Envelopes for the Steering System

In order to reduce material susceptibility to high stresses, care must be exercised when defining operational envelopes. The primary purpose of the study was to show that tip maneuvering is possible, i.e., one can switch the mode of operation at will and guide the penetrometer tip towards a known target. This task has been successfully accomplished, demonstrated, and summarized in the Phase I final report [1]. The task of this phase was to describe guidelines and operational boundaries. The description includes penetrometer rod and tip modeling based on the semi-passive tip design selected and tested in Phase I.

The ability to predict the behavior and performance of the penetrometer system will provide a useful tool for future designs. Preliminary computation of the force-couple and the resulting maximum stress distribution along the rod, lays the foundation for a preliminary determination and evaluation of the system's operational envelope. Examination of the rod path profile is needed in order to identify zones where stresses may present a problem. Most severe bending stresses occur at sections of minimum radius of curvature. Most severe axial stresses, due to "push" forces, occur at the highest rod segment near the insertion point. Combination of these two factors will determine the locations where stresses of maximum intensity occur. Care must be exercised when stress conditions are determined and compared to their allowable values.

Critical stresses may be identified along the penetrometer rod in several locations. Some of these stresses are associated with large axial force, others are found in segments with small radius of curvature, however, the most susceptible elements in the entire rod system are the rod joints. Not only can the joints be under the influence of a large axial force and a small bending radius of curvature, additional torque, applied to the rod to activate or deactivate its directional tip, will induce hoop stresses at the joint conical thread. The locking ring of the steerable joint will prevent loosening of the joint when steering torques are applied to penetrometer rods.

A useful tool for definition of operational envelopes of the steering system is a simulation (analytical) model. To enhance simplicity, the analytical model used in this simulation represents a two dimensional domain based on incremental insertion of a penetrometer rod equipped with a directional wedged tip. For the study at hand, the steerable tip tested in Phase I (Figure 1) was selected. The tip can be inserted into the ground either in its symmetrical-passive or asymmetrical-active configuration. Switching the steering mechanism from passive to active mode is accomplished by a half-turn of the rod counterclockwise to activate, and clockwise to deactivate.

Details of the simulation model are discussed in the Appendix. In summary, the model treats the penetrometer rod string as a series of cantilever beams and applies the "simple beam theory" [1] to each beam segment. This leads to calculation of the rod trajectory and the resulting radius of curvature, and normal force distribution along the penetrometer rod string. The results can then be used to define the operational envelopes of the steering system.

For a quantitative evaluation of the system's operational envelope, a penetration of 100 feet was selected. The penetrometer rods are inter-connected by the steerable joints designed in Phase

I. The first rod is equipped with the passive-active steering tip attached to its lower end by a similar joint. Based upon the rod and soil parameters mentioned in the Appendix, Figure 8 displays the penetrometer rod trajectory, while Figure 9 shows the normal-axial force distribution.

The rod trajectory shown in Figure 8 shows lateral deflection of penetrometer rods as a function of penetration depth. The tip command polarity indicates that the rods were pushed with the steering tip in its steering mode from the beginning of the push. The results indicate that a lateral reach of 40 feet is possible over a length of push of 100 feet.

In practice, friction reduction rings with slightly larger outer diameter than that of penetrometer rods are mounted along the rod at 3 to 4 foot increments. Because of their larger diameter, the rings create a gap between penetrometer rods and the soil, resulting in a reduction of skin resistance. This results in a reduction of forces needed to push penetrometer rods into the ground. The magnitude of force reduction varies as a function of the soil type. However, in numerous field tests with friction reducing rings, it has been observed, empirically, that the rings reduce the pushing force by up to a factor of 4.

In Figure 9, the distribution of normal force in penetrometer rods is shown as a function of penetration depth. Two curves are shown in this figure. The dashed curve is for penetrometer rods equipped with friction reducing rings, whereas the solid curve is for bare rods. From this figure it is observed that the normal force increases towards the ground surface and can reach up to 52,000 lbs in bare rods. In rods equipped with friction reducing rings, if one assumes a four fold reduction in skin resistance, the normal force in penetrometer rods is reduced to 13,000 lbs.

The local radius of curvature along the penetrometer rods of Figure 8 is shown in Figure 10. The radius of curvature by definition is the second derivative of the path. Therefore, the curve in Figure 10 was computed via two successive numerical differentiations of the rod trajectory Y(X) of Figure 8. The results indicate a fairly constant radius of curvature of 119 feet. The curvature will change as a function of the soil type and the steering tip configuration.

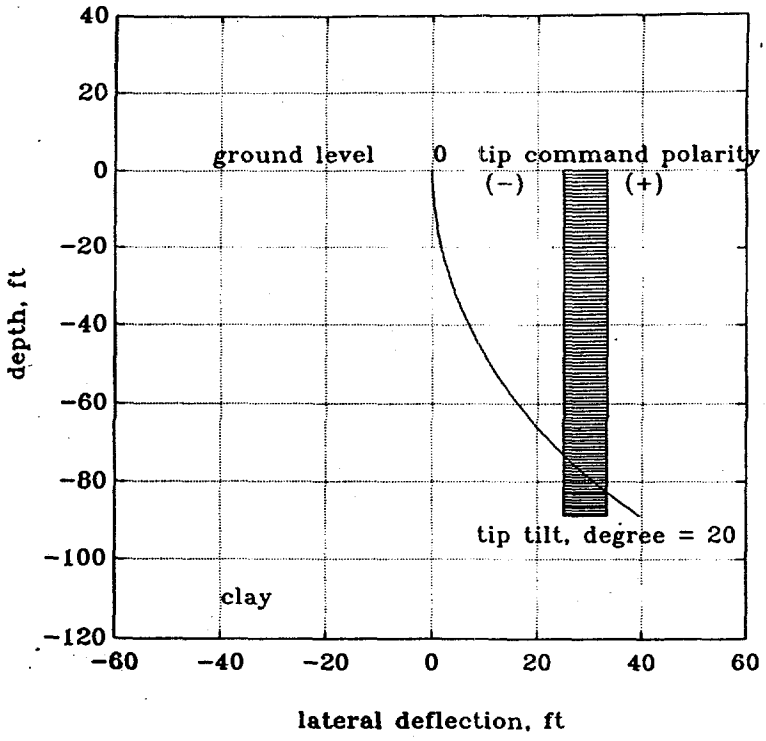

Figure 8. Simulated penetrometer rod trajectory.

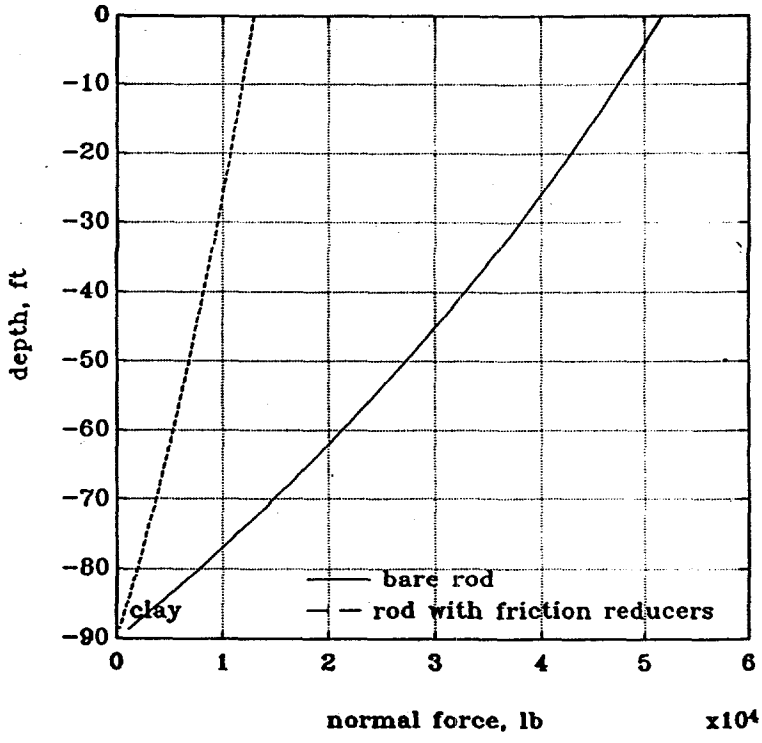

Figure 9. Simulated normal-axial force distribution.

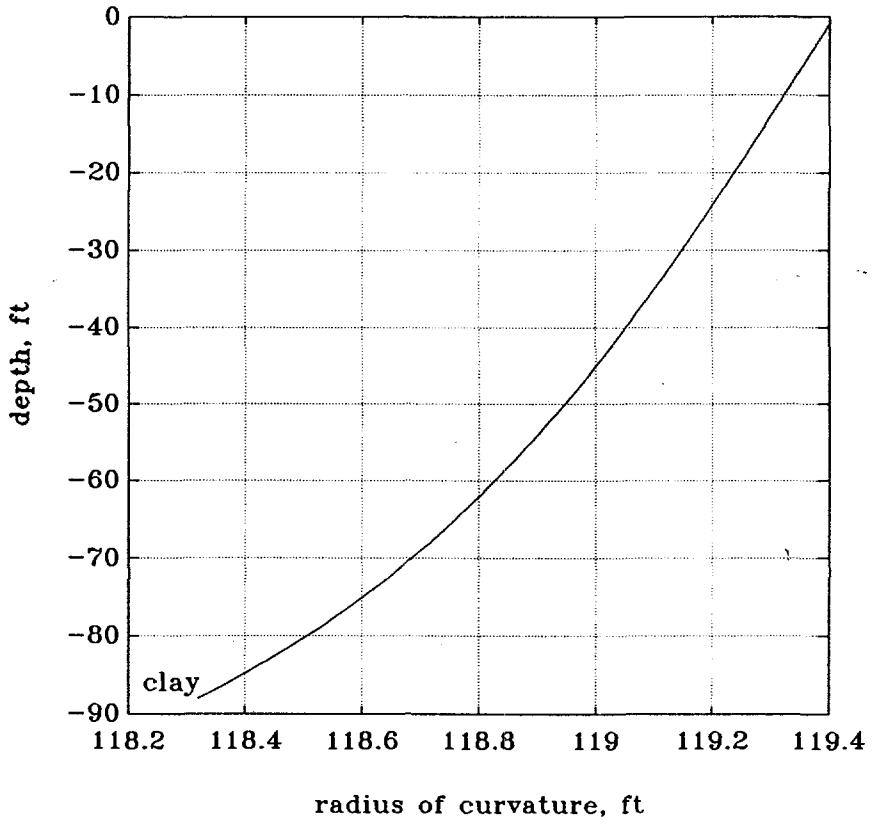

Figure 10. Simulated local radius of curvature.

The combined maximum normal compression stress along the rod due to the normal-axial force N and the resulting bending, expressed by the radius of curvature, may be computed point-wise by the following expression:

$$\sigma_{max} = \frac{ED}{2\rho} + \frac{N}{A} \qquad (1)$$

In this expression, E is the rod material modulus of elasticity, D is the external diameter, A is the cross-sectional area, ρ represents the rod local radius of curvature (second derivative of the path), and N is the axial force. The maximum normal stress along the rod was computed at two typical locations, one at the outer surface of the rod while the other at the outer surface of the thread base. D and the associated A in Equation (1) were substituted accordingly. Figure 11 displays the resulting computations. Evidently, the stress at the joints is higher. The global maximum stress (the maximum σ_{max} along the entire path of Figure 8) at the joint reached 63,000 psi (15,000 psi due to bending and 48,000 psi due to axial force) while 49,000 psi only at the outer surface of the rod.

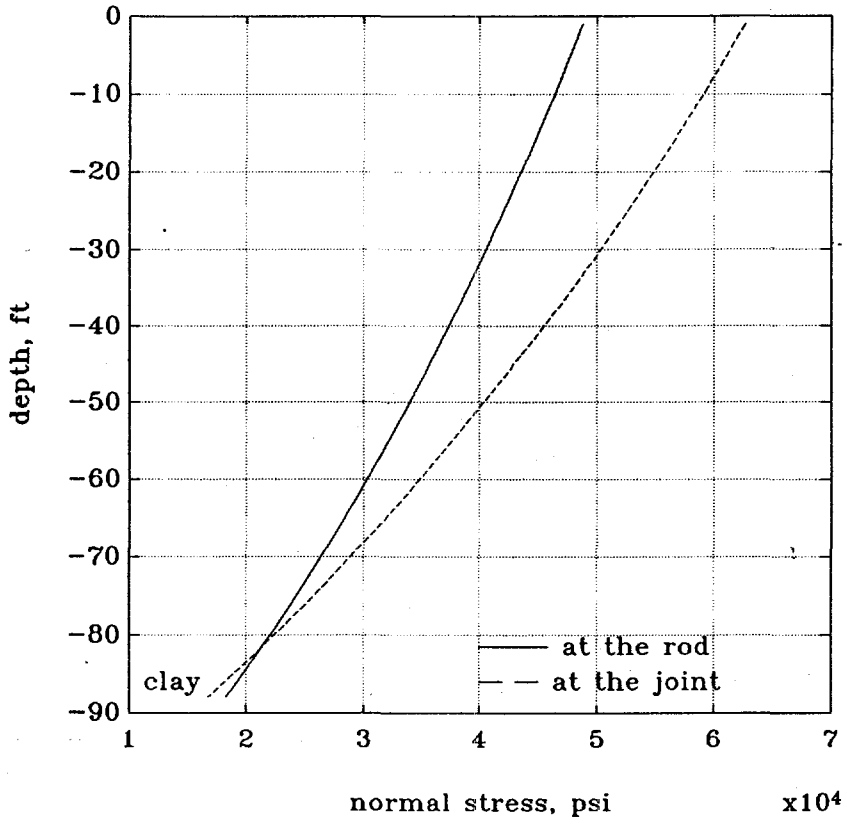

Figure 11. Simulated maximum normal stress.

The simulation shown in Figure 11 assumes only normal and bending stresses. A third stress component that was not considered in Equation (1) is the torsional stress due to torque influences while pushing rods into the ground. The META-DRILL used for pushing rods into the ground, unlike standard penetrometer trucks does not firmly grip the rods at the surface while pushing. This allows semi-free rotation of the rods under torque influences and a reduction in torsional stresses. On the other hand to activate or deactivate the steering tip, a large torque is applied to the rods at the surface, while the pushing mechanism is disengaged. In this case, torsional stresses in the rods are high, but normal stresses in the rods are reduced to zero.

Tip activation or deactivation command is transmitted via a half turn of the entire penetrometer rod. For this purpose a torque is applied to the penetrometer rod at the surface by a torque mechanism. Similar to Figures 8-11, Figure 12 is a computer simulation that displays the torque distribution along the 100 ft long rod due to this process. Normally, the rod shoving operation is interrupted at the time of rotation. According to the figure, a torque magnitude of 46,500 in-lb is needed in order to rotate the entire rod in clay.

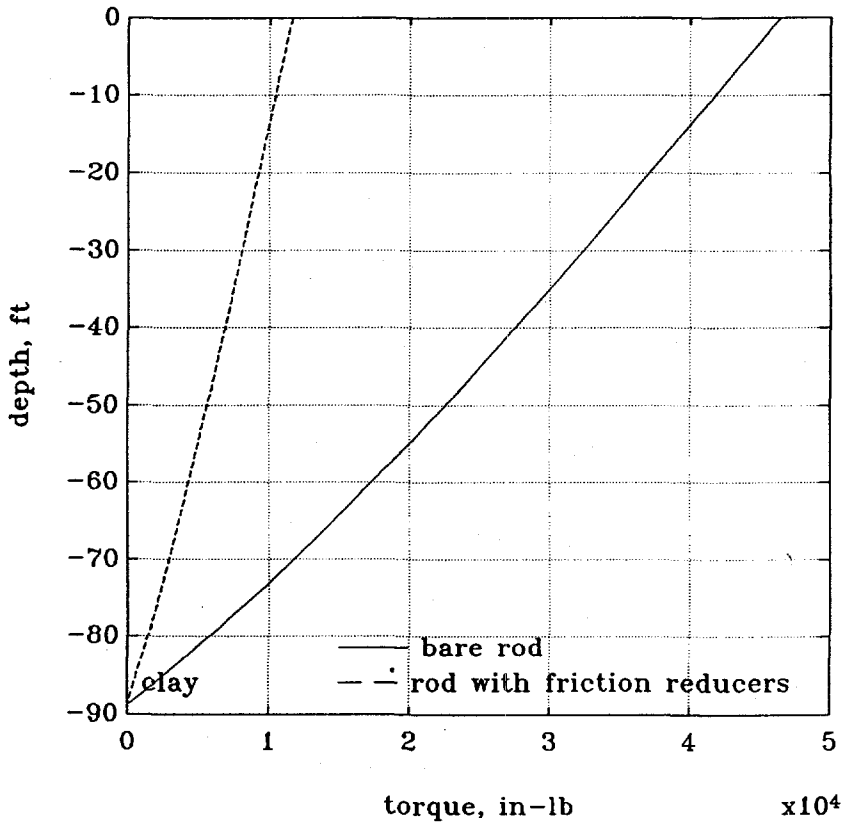

Figure 12. Simulated torque distribution.

Using friction reducing rings the torque needed to rotate the rod may be reduced by a factor of 4. Based on Figure 12, a torque magnitude of 11,600 in-lb will be needed when friction reducers are used. The resulting maximum shear stress in the joint area due to this torque may be computed using the following expression:

$$\tau_{max} = \frac{T D_0}{2J} \qquad (2)$$

where T is the applied torque, D_0 is male thread base outer diameter, and J is the cross-sectional polar moment of inertia. For the given torque and joint cross-sectional geometry, the maximum shear stress obtained was 19,700 psi.

A preliminary joint tightening by a torque of about 8,000 in-lb is needed prior to field operation in order to maintain the joint torque capacity. The pre-tightening torque results in 38,300 psi hoop stresses in the joint walls of the male part. Figure 13 displays the state of plane stress at the joint. In the figure, σ_b is the maximum normal stress due to bending only, σ_t is the joint hoop stress, and τ represents the maximum shear stress. Computation of the principal (absolute maximum) stress at this point revealed a stress level of 50,000 psi.

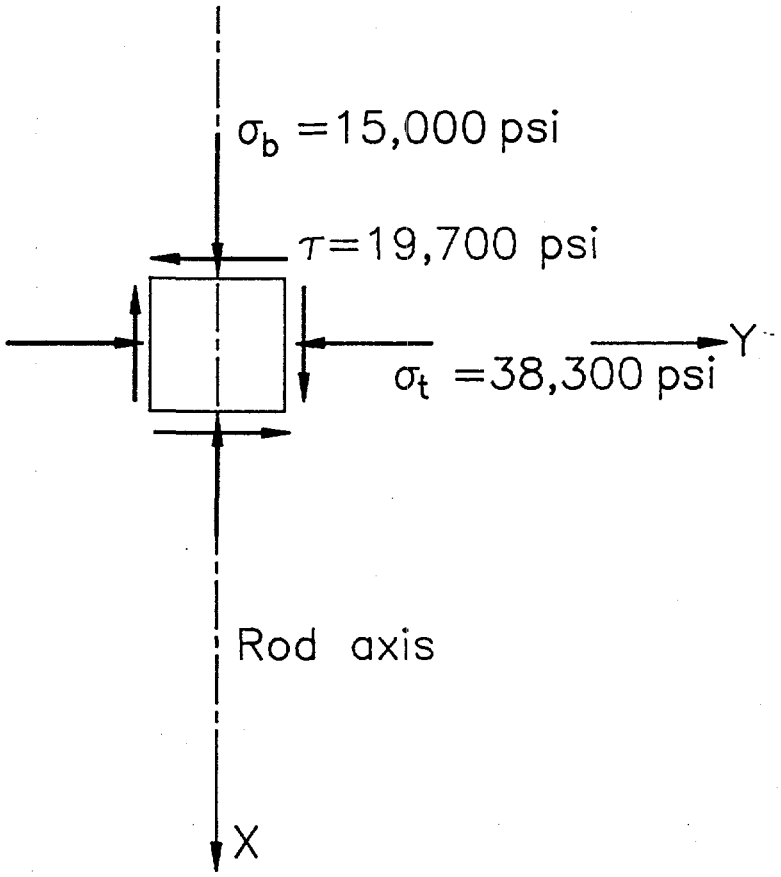

Figure 13. State of stress at the joint.

In summary, an operational envelope may be constructed in order to identify the available range for the normal-axial force N, and the radius of curvature ρ. The determination of this operational zone is based on a relationship between N and ρ. Let N be the current axial force at a point along the rod, ρ its associated radius of curvature, and σ_{allow} the rod material allowable stress, this axial force may be increased up to a maximum level N_{max} according to equation 3:

$$N_{max} = N + \left[\sigma_{allow} - \left(\frac{ED_0}{2\rho} + \frac{N}{A_{joint}} \right) \right] A_{joint} \qquad (3)$$

As may be concluded from Figure 11, the joints are under higher stress level with a maximum at the ground level. Therefore, the determination of the operational zone is based on the joint geometry where D_0 is the joint male thread base diameter and A_{joint} its cross-sectional area. The area to the

left of the curve in Figure 14 (a) represents the N-ρ operational envelope for rod material with ultimate stress of 120,000 psi and allowable stress of 60% of ultimate. Figure 14 (b) is an enlargement of the lower left portion of Figure 14 (a). For a large radius of curvature, when ρ approaches infinity, $N_{max} = \sigma_{allow} A_{joint}$, representing the joint axial force limit, as shown in Figure 14 (a). On the other hand, since the lowest value that N_{max} may assume is the current value N, the lowest value that ρ may assume is the one that will nullify the term in the brackets.

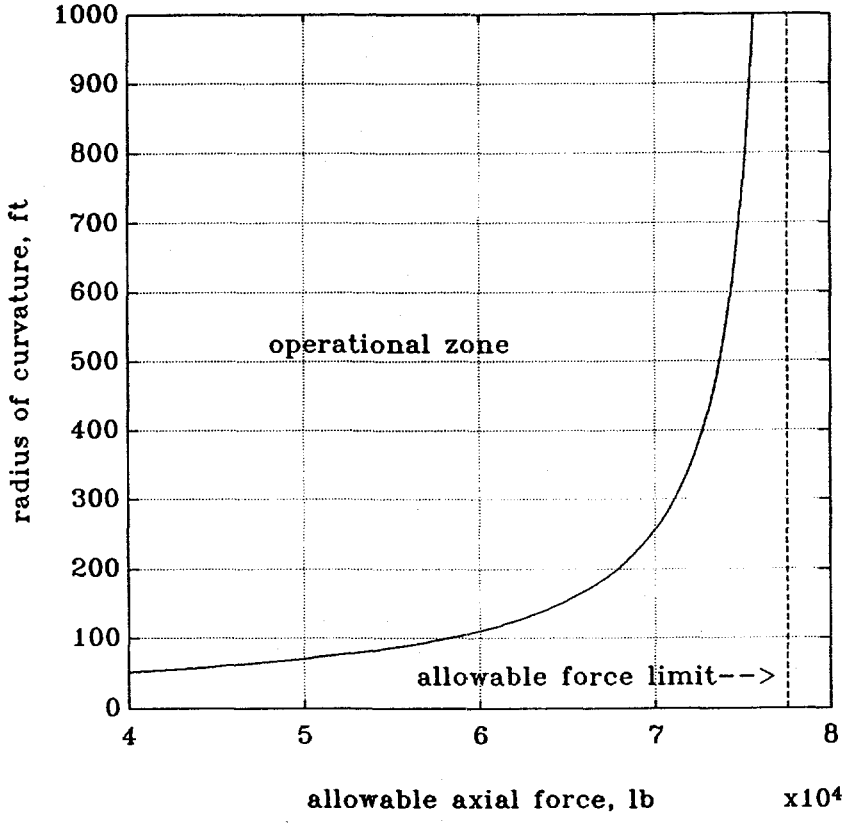

(a) Full range.

Figure 14. The N-ρ operational envelope.

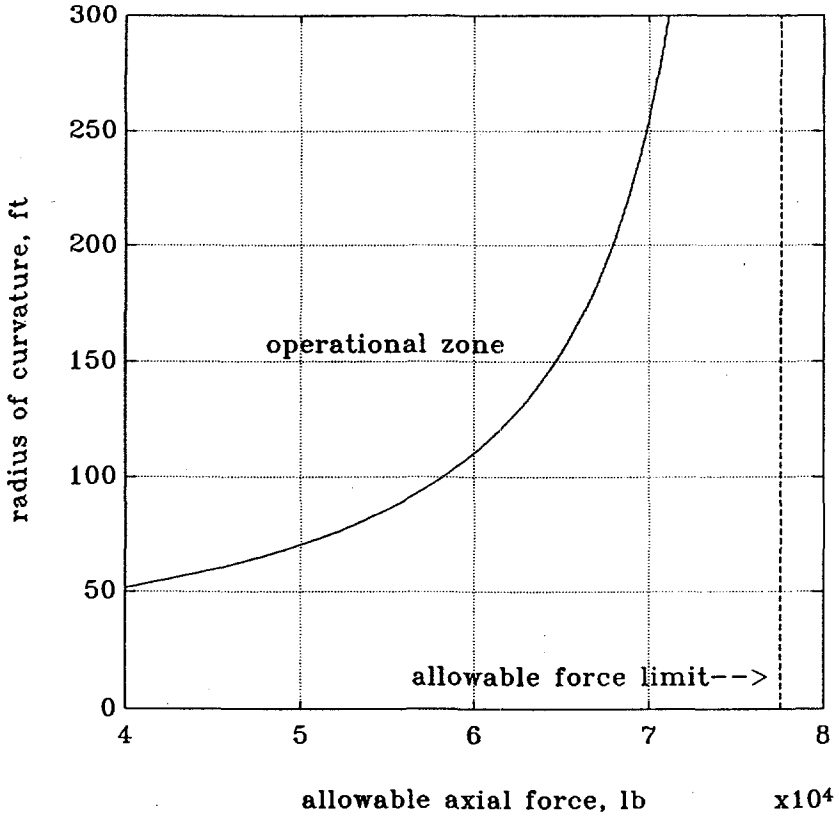

(b) Enlargement of lower left portion of Figure 14 (a).

Figure 14. The N-ρ operational envelope.

2.2 Operational Envelopes for the Vibratory/Thrusting Systems

The META-DRILL shown in Figure 4 provides the vibratory/thrusting penetration capability. Vibratory pushing is provided by a vibratory head. Vibrations are generated when a single unbalanced mass is rotated inside the vibratory head. A hydraulic motor attached to the head provides the means for rotation of the mass. The frequency of vibrations can be varied by varying the flow of hydraulic fluid to the motor. The amplitude of vibrations can be adjusted by opening the head and adjusting the configuration of the unbalanced mass. In addition to vibratory pushing, penetrometer rods may be pushed into the ground by thrusting the rods using the drive chains and the META-PRESS of the rig. Figure 15 is a closeup view of the vibratory head and the drive chain.

Figure 15. Closeup view of the vibratory head and the drive chain.

Based on META-DRILL specifications the operational envelopes of the vibratory/thrusting systems are:

Vibratory Drive

- maximum of 7,500 lb centrifugal force
- variable frequency. Maximum 200 Hz

META-PRESS

- 5 foot strokes
- maximum down force of 6,000 lbs
- maximum pull back force of 6,000 lbs

2.3 Operational Envelopes for the POLO system

The POLO system which is the navigational unit of the overall system is made up of downhole and uphole components. The downhole components include the POLO rod module and a downhole data acquisition package. The POLO rod module has been designed to measure bending strains of up to 1000 $\mu\epsilon$ (micro-strain) at the level of strain gages. Considering the geometry of the POLO rod module, a measured strain of 1000 $\mu\epsilon$ corresponds to a radius of curvature of 55 ft. Regarding the magnitude of thrust that can be applied on the POLO rod as a function of curvature of the path, Figure 14 which was developed for penetrometer rods may be used safely.

An important operational envelop for POLO in vibratory applications is the number of vibrations that the strain gages can be subjected to before fatigue failure. The most important factor that determines the fatigue lifetime is the magnitude of the applied stress or strain amplitude. Fatigue life increases as the amplitude is decreased, until a certain stress or strain level is reached below which fatigue will not occur under unlimited cyclic vibrations. Care was exercised to select strain gage components so that they can undergo unlimited cyclic vibrations without fatigue failure as long as the strains are kept below 1000 $\mu\epsilon$. In order to reduce the risk of fatigue failure in the field, POLO strain readings will be monitored carefully. Operations will stop whenever strain levels go over 1000 $\mu\epsilon$ for an extended period of time.

2.4 Operational Envelopes for the Anchoring System

The operational envelope for the anchoring system is to provide at least 6,000 lbs of pull-out capacity under vibratory conditions. Under task 2.3 an anchoring concept based on screw anchors was tested in the field. Details regarding the test results and concept refinements are presented in Section 4.2.

3.0 FULL-SCALE STEERABLE SYSTEM INTEGRATION

The steerable system includes the steerable penetrometer tip, rod joints suitable for curved paths, and a torque mechanism for application of joint tightening and steering torques to penetrometer rods. Under task 2.2 each of these systems was analyzed and redesigned when necessary for integration into the overall full-scale penetrometer system. The penetration simulation model and the operational envelopes of Section 2, along with laboratory and field test results of Phase I were utilized in this task.

3.1 Steering Tip

The operational envelope for the steering tip shown in Figure 10 was deemed adequate for the full-scale system. The operational envelope was deemed adequate, because the average radius of curvature of 119 feet provides the means for the META-DRILL to be anchored next to a building or an underground storage tank with the purpose of pushing rods towards targets underneath these structures.

In order to integrate the steering tip with the full-scale system, the steering tip has to be securely connected to the POLO rod module. The connection between the steering tip and the POLO rod has to withstand the steering torque transmitted to the tip, the axial pushing force, and the stresses due to bending around a curved path. As shown in Figure 12 the steering torque decreases substantially from those applied at the surface. The same is true for axial pushing force (Figure 9). Therefore, one option that was considered for the steering tip-POLO connection was to use steering joint threads without the locking mechanism. For this option, in order for the connection to resist the steering torques, the joint had to be pre-tightened with a torque larger than that due to steering. However, because of uncertainties in the magnitude of the steering torque and the consequences of the connection opening under vibrations, it was decided to equip the steering tip-POLO connector with the same locking ring used for penetrometer rods. It is believed this will minimize the risk of losing the steering tip downhole or damaging the POLO rod module.

3.2 Steerable Rod Joints

The performance of the steerable rod joints designed and tested in Phase I (Figure 2) was compared with the required operational envelopes and they were deemed satisfactory. However, during the field tests of Phase I, working with the locking mechanism was observed to be difficult and time consuming. Because in full-scale operations tens of these locking joints have to be assembled in the field, it was decided to redesign the locking mechanism.

To test the assembly and performance of the redesigned joint, one unit was manufactured and lab tests were performed at UTD. Regarding the ease of assembly, it was determined that the redesigned locking joint was much more user friendly. Unlike the original design, the parts of the redesigned joint did not have to be aligned accurately prior to assembly, and no special tools were needed for assembly. Timewise, it takes essentially the same amount of time to assemble the redesigned locking joint as it takes with off the shelf joints.

Laboratory torque tests at UTD indicated that the locking mechanism could withstand torque levels of up to 10,000 in-lb before loosening. The prototype locking mechanism that was tested at UTD was made of normal steel. It is the intent to make the penetrometer rods and their locking joints of high strength steel during full-scale tests. This will allow application of larger torques for steering purposes.

In addition to laboratory torque tests, bending tests were performed on the redesigned locking joint. In these tests a rod with the redesigned locking, steerable joint was tested in a simple support frame with a concentrated load applied half way between the two supports. The magnitude of the load was monitored by a load cell and deflections were measured with a dial gage. The main purpose of the test was to determine how far the rod could be bent before the onset of failure. Figure 16 shows the results of the bending tests. According to this figure, the steerable joint essentially behaves in a linear fashion up to a deflection of 0.19 in. which is equivalent to a radius of curvature of 32 ft. On the other hand the commercial penetrometer joint tested in Phase I had an initial dog leg at 85 ft radius of curvature (0.07 in deflection). Laboratory bending tests in Phase I also included a plain rod without any joints. As shown in Figure 16, the curve for the redesigned locking joint and the plain rod are nearly identical.

The equation used for conversion of deflection to radius of curvature is:

$$r = \frac{\ell^2 + 4d^2}{96d} \qquad (4)$$

where r = radius of curvature (ft),
ℓ = distance between simple supports in the test frame = 24 in, and
d = deflection (in).

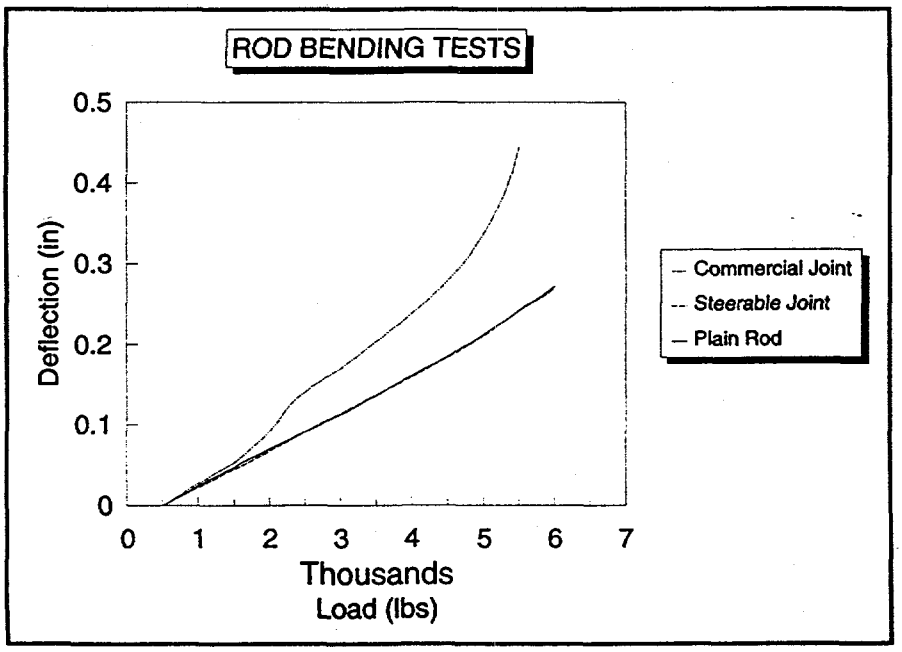

Figure 16. Results of bending tests on redesigned steering joint.

3.3 Steering Torque Mechanism

A torque mechanism is needed for the full-scale penetrometer system. One use of the torque mechanism will be for pre-tightening of the steering joints. Another use will be for application of torque to change the mode of operation of the steering tip. Figure 10 was used as a guideline in design of the torque mechanism. The design was carried out on a preliminary level in Phase I. In Phase II, the design was finalized for integration with the full-scale penetrometer system.

The designed mechanism for application of steering torques is shown in Figure 17. The mechanism consists of two pipe wrenches tied to each other by a hydraulic cylinder. For steering applications the wrench on the left (fixed wrench) will be tightened against a fixed rod which is welded to the frame of the META-DRILL. The wrench on the right (steering wrench) is then tightened against the penetrometer rod just above the ground. Steering torque is applied by activating the hydraulic cylinder which pulls the handle of the steering wrench to the left. Depending on the type of soil, up to a certain depth of penetration, this results in clockwise turning of the entire penetrometer rod string. In medium dense, sandy clay soils the length of rods that can be turned from the surface using the torque mechanism is expected to be 100 feet. In a worst case scenario, if the rods can't be rotated, the penetrometer rod string may be pulled out entirely so that the mode of operation of the steering tip can be changed at the surface.

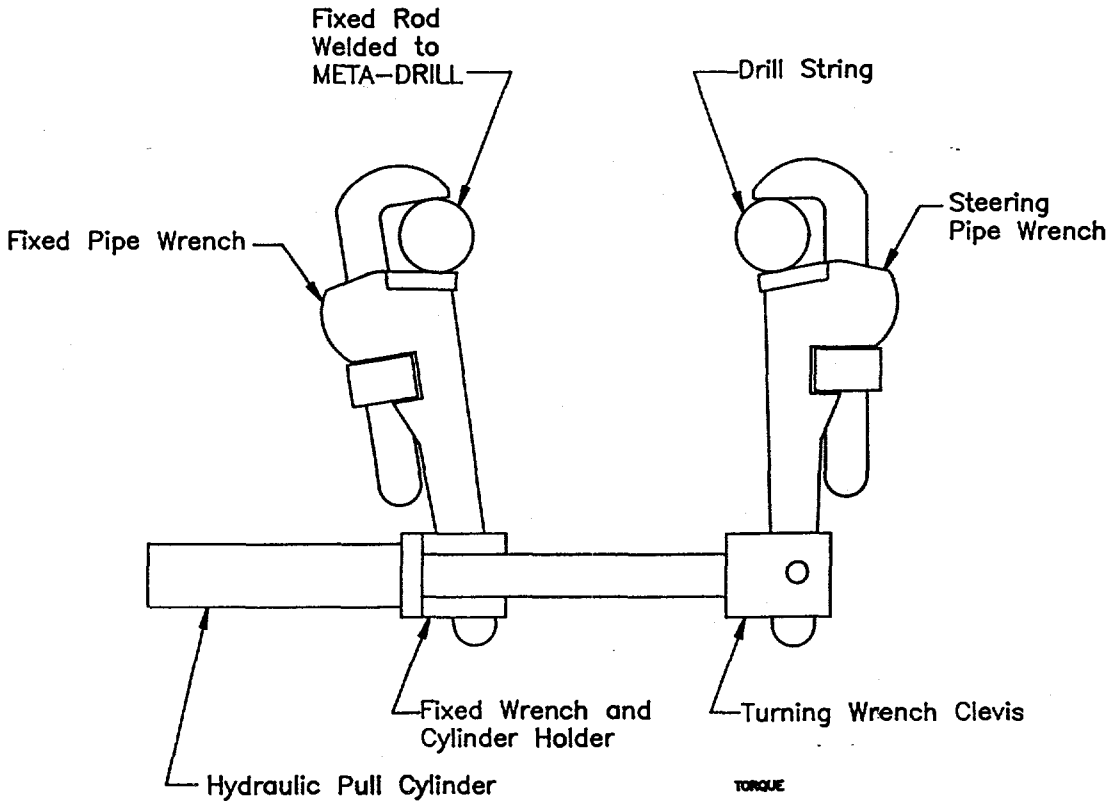

Figure 17. Steering torque mechanism.

4.0 FULL-SCALE META-DRILL STEERABLE SYSTEM INTEGRATION

META-DRILL is the main platform for the full-scale steerable penetrometer system. In addition to integrating the steering systems (discussed in Section 3), the POLO and the anchoring systems have to be integrated with the META-DRILL. Figure 18 shows the entire full-scale integrated system.

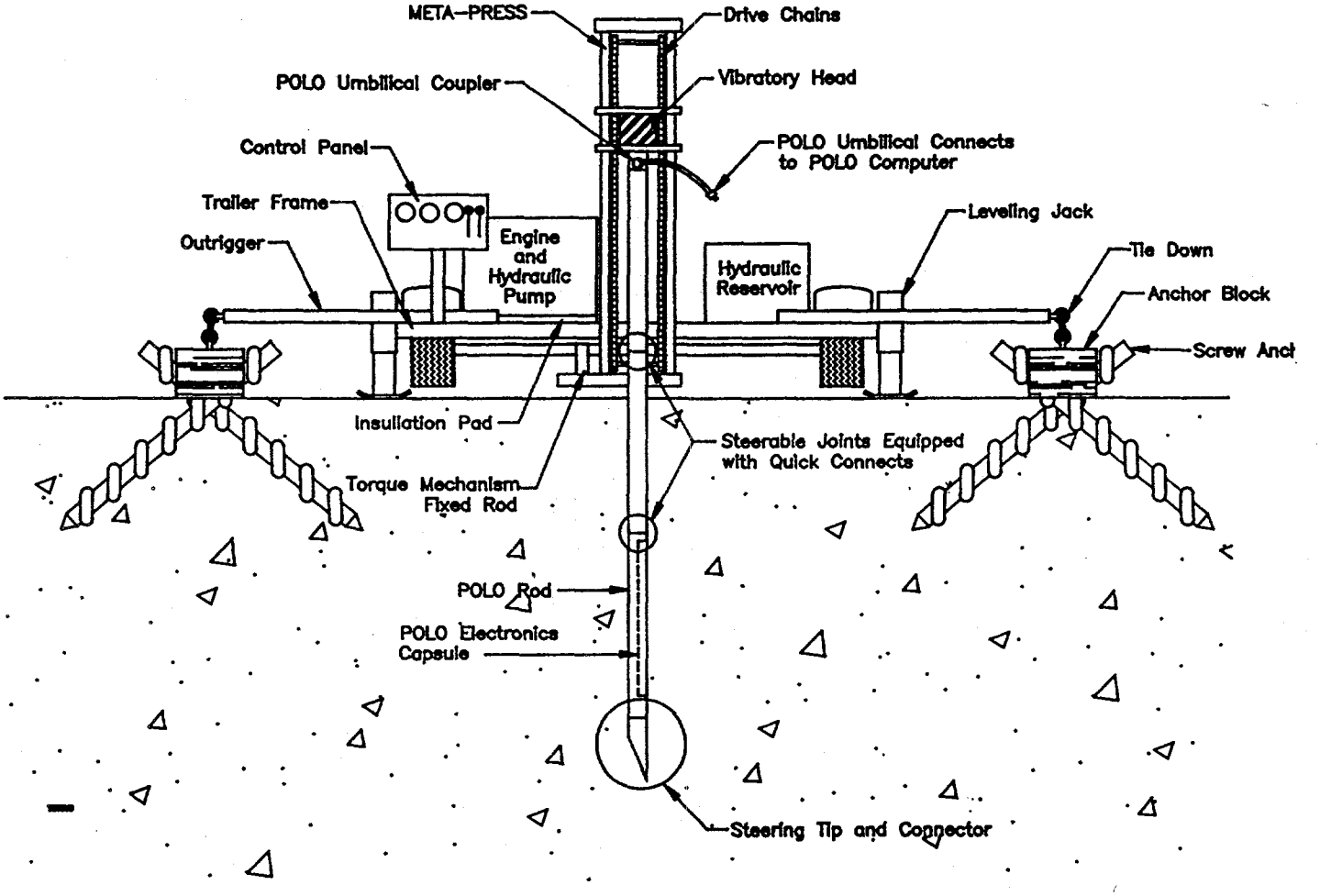

Figure 18. Integrated full-scale penetrometer delivery system.

4.1 POLO System Integration

Integration of the POLO module involves the POLO rod and its downhole electronics. The POLO rod has one end adapter at each end. In manufacturing commercial POLO rods, the end adapters are designed to match the threads of the penetrometer rods used by the customer. To integrate POLO with the steerable penetrometer, the end adapters will be similar in design to the redesigned steerable locking joints.

The downhole electronics (Data AcQuisition, DAQ) of POLO is housed in a sealed capsule that fits inside the inner space of the POLO rod. Figure 19 shows the space occupied by the capsule. For the META-DRILL applications, the capsule design was reviewed and modified to reduce shock loading to downhole components. The modification included added padding around the components and a more secure tie down of the electronic boards and batteries.

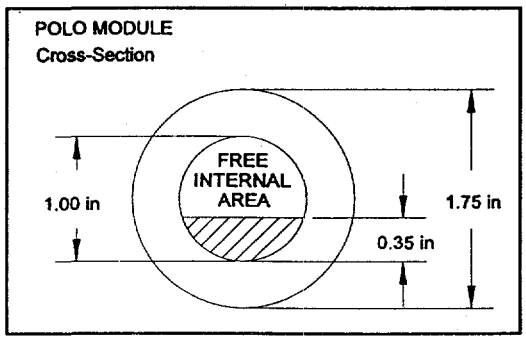

Figure 19. DAQ capsule inside the POLO rod (cross hatched).

A two conductor umbilical carries the signal from the DAQ package to the surface computer. The same umbilical is used to power the DAQ and the strain gages of the POLO rod. A concept called Quick-Connects was adapted and tested on a preliminary level for use with the META-DRILL system in Phase I. This concept involves using the penetrometer rods as one conductor and a male and female Quick-Connect at each end of the penetrometer rods. An insulated wire, spot epoxied inside each penetrometer rod makes electric connection between the male and female Quick-Connects, thus providing for the second conductor of the DAQ package. Figure 20 (a) shows the male and the female parts of a Quick-Connect. An assembled Quick-Connect is shown in Figure 20(b). As shown in this figure, electrical connection is made as soon as the penetrometer rod joint is tightened. The tests in Phase I included building Quick-Connect mockups and transmitting a known signal through 14 penetrometer rods. The received signal was analyzed to ensure signal integrity.

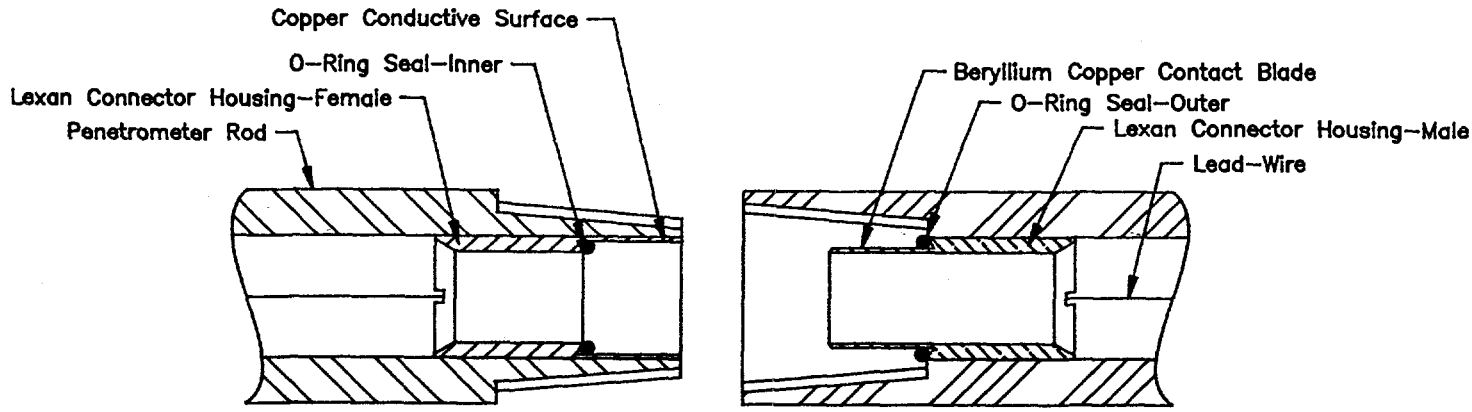

(a) The male and the female parts of a Quick-Connect.

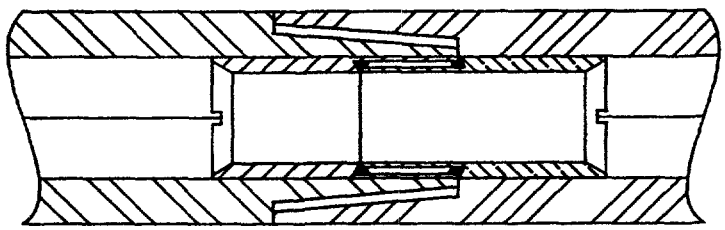

(b) An assembled Quick-Connect

Figure 20. Schematics of the Quick-Connect Concept.

Two factors were studied and designs were made for integration of the Quick-Connect concept with the META-DRILL. The first factor was the connection between the last Quick-Connect at the surface and the POLO umbilical that runs to the surface computer. It was necessary to design a POLO umbilical coupler with a Quick-Connect at its male end and a hole drilled on its side just large enough for passage of a short length of insulated wire attached to the Quick-Connect as shown in Figure 21. The end of this wire along with the end of a second insulated wire soldered to the outer surface of the coupler are sealed inside a plug type connector (shown in Figure 21). This way, after each penetrometer rod is assembled, the POLO umbilical coupler makes the physical connection between the last rod and the vibratory head, and also provides the electrical connection for the POLO umbilical.

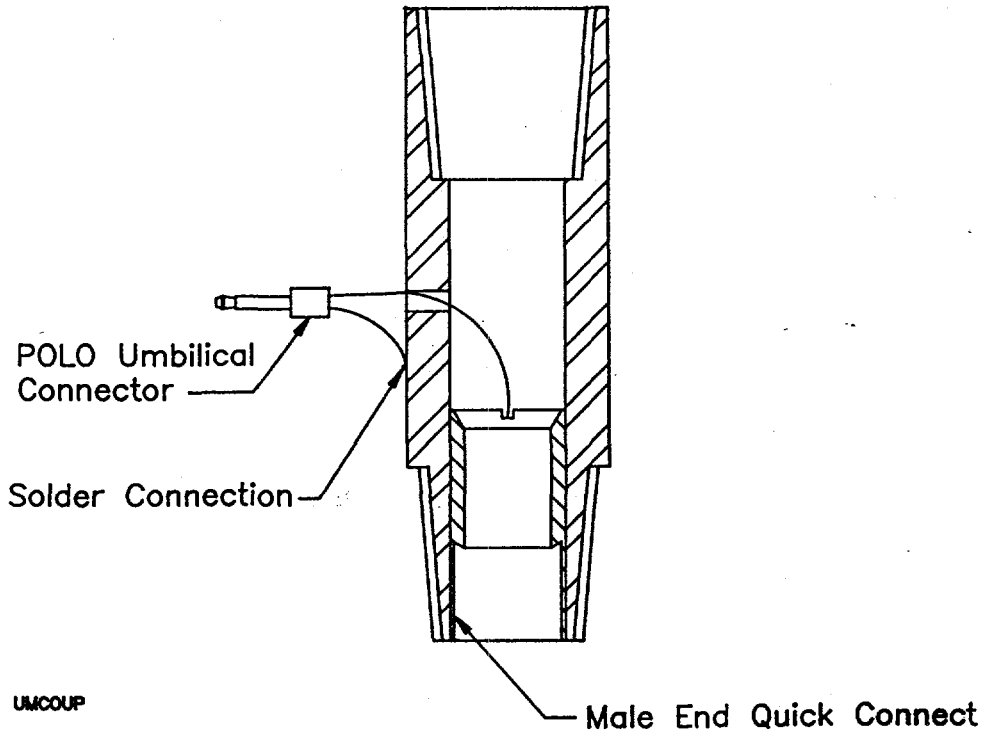

Figure 21. POLO umbilical coupler.

A second factor that was considered in integration of the Quick-Connects with the META-DRILL was insulation of the DAQ signals from the META-DRILL engine and its battery. The META-DRILL system is modular, with the engine and hydraulic pump as one module housed in a small frame which in turn is mounted directly on the chassis of the META-DRILL. A simple method of insulation is to use polyethylene padding at critical locations as needed. One critical location shown in Figure 18 is between the hydraulic pump and the chassis of the META-DRILL.

An alternative method to insulation padding was to use a strong non-metallic material for the housing of the POLO umbilical coupler shown in Figure 21. However, this was deemed not practical and more expensive.

4.2 Anchoring System Integration

The hydraulic press (META-PRESS) of the META-DRILL has a 6,000 lb push capacity. However, due to its light weight, the META-DRILL can only apply approximately 1,500 lbs before it lifts off the ground. To overcome this problem, an anchoring system which had been devised and tested to a limited scale in Phase I was tested during Phase II to determine its capacity. Figure 22 shows the anchoring system and its setup during the Phase I tests. It consisted of a pair of screw anchors driven into the ground manually and attached to the META-DRILL by rope.

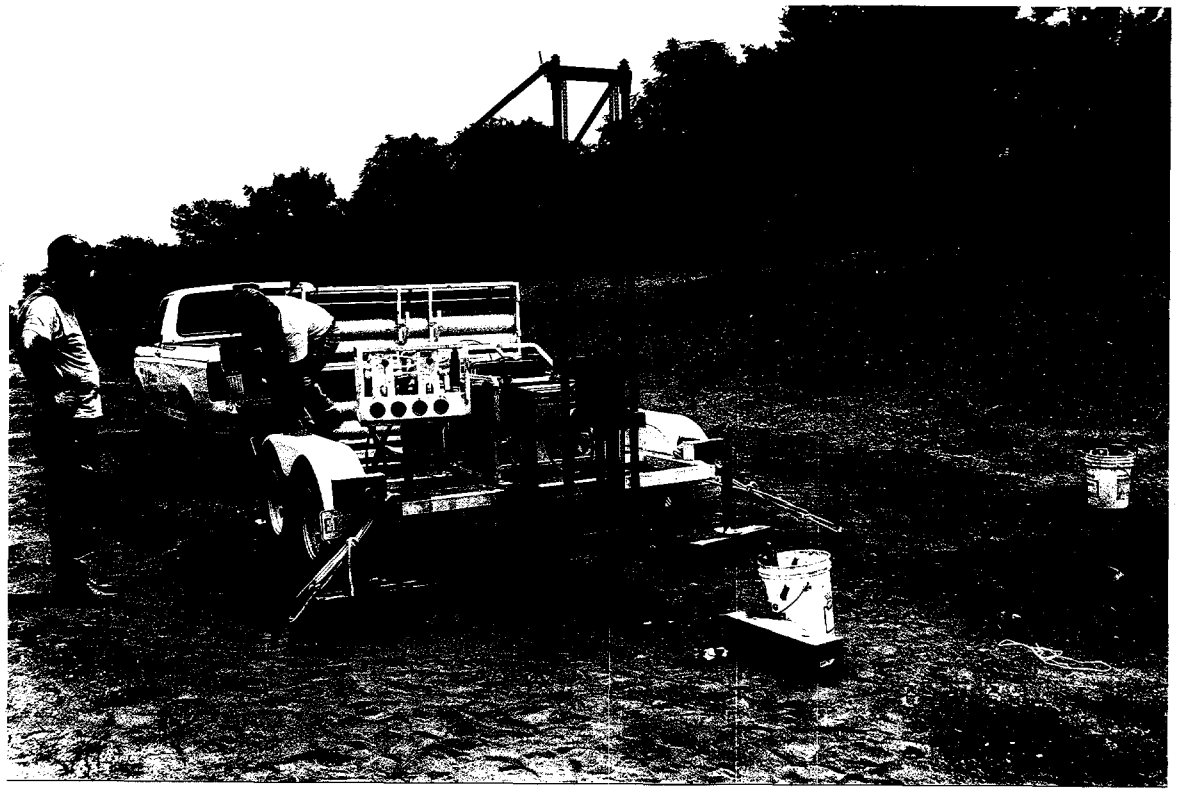

Figure 22. Field testing of screw anchors.

In the field tests of Phase II a load cell was used in the penetrometer string to measure the pull out capacity of the anchoring system. Two sets of tests were carried out. In the first set, only the META-PRESS was used with the vibrations off. At the end of the test the load cell registered a force level of 4,200 lbs and the anchors remained in place. The test was ended because the META-DRILL could not apply a larger thrust. It is believed the cause for not being able to push up to the maximum of 6,000 lbs was that the engine and the hydraulic pump of the META-DRILL had not been tuned for optimum performance before the tests. The tune up and adjustments for optimum performance are an integral part of the full-scale system assembly task of Phase III.

In a second set of tests, the vibratory head was turned on after the META-PRESS had reached its capacity. The rope attachment performed satisfactorily, but the sudden start of vibrations caused one of the anchors to pull out of the ground.

Based on observations of the field tests of Phase II, a more robust anchoring system was designed. This is shown in Figure 18. In the new design, instead of using only one screw anchor on each side of the rig, two angled anchors connected to an anchor block are utilized. In addition, an outrigger is installed on each side of the rig to allow for lateral relocation of the anchors, if screw anchors hit a cobble which prevents further screwing of the anchors into the ground. The screw anchors will be placed in the ground using a hydraulic motor. This will allow for rapid placement of the anchors. The anchoring system shown in Figure 18 is expected to perform satisfactorily in most soil formations including very sandy soils. The tests carried out on the anchoring system in Phases I and II were carried out in a sand quarry.

5.0 PLANS FOR FULL-SCALE INTEGRATION AND FIELD TESTING

The Phase II effort was essentially a preparatory phase in order to get ready for full-scale field tests that will be performed in Phase III. The main objective of the full-scale field tests is to show that the full-scale system can be used in the field to push the tip of the penetrometer to a known location within the reach of the system. The reach of the system is the outer limit of the underground region that can be reached with the pushing capability of the META-DRILL and the steerable tip tested in Phase I.

Before any full-scale field testing is carried out, all of the full-scale sub-systems will be manufactured and assembled at the start of Phase III work. They include a steering tip, a POLO system, Quick-Connects, penetrometer rods equipped with steering and locking joints, and an anchoring system. After the assembly of the sub-systems, several shake down tests will be carried out. The tests will include the META-DRILL to ensure optimum performance setting of the engine and the pumps, the redesigned locking joint, the POLO and the Quick-Connects, and the anchoring system. The shake down tests will be carried out at sites local to UTD.

After completion of the shake down tests, field tests will be performed to demonstrate the steerability and penetrability of the integrated full-scale system. In order to check for system performance regarding steerability, POLO readings will be compared with target coordinates set before each test. For repeatability, at least two tests will be performed for each predetermined target. Several targets will be used in varying soil formations.

The tests for quantification of the effects of vibrations will be carried out with the META-DRILL and a standard penetrometer truck. Depths of penetration from META-DRILL will be compared with those achieved using a standard penetrometer truck. The truck will be operated at a force level equal to the sum of static and dynamic pushing capability of the META-DRILL which is on the order of 14,000 lbs.

Initially, the field tests of the full-scale system will be carried out at sites local to UTD. After debugging of these tests, plans will be made for field testing of the full-scale system at government facilities. Under the first task suitable sites for field tests of Phase III will be selected.

In summary, the tasks of Phase III effort are:

Full- Scale System Integration and Field Testing

Task 3.1 Environmental Work

Select uncontaminated sites for full-scale field testing. In addition a test plan will be developed to include details of shakedown tests and the general requirements for full-scale field demonstrations at government facilities. The general test plan will be refined further depending on the sites selected for full-scale demonstrations.

Task 3.2 Steerable System Manufacturing

Manufacture and assemble the steerable system. The components to be manufactured include steering tips, steerable joints, and a torque mechanism.

Task 3.3 Vibratory Penetrometer System (VPS) Manufacturing

Manufacture system components and assemble a field deployable VPS. META-DRILL is the major component of the VPS. This unit was purchased in Phase I. Under this task, the META-DRILL will be outfitted with an anchoring system. In addition, a shock resistant POLO system will be manufactured and assembled.

Task 3.4 Field Testing

Perform full-scale field tests according to the test plan of task 3.1.

Task 3.5 Reporting

Summarize the results of tasks 3.1-3.4 in a final report for Phase III.

6.0 CONCLUSIONS

The work summarized in this report has led to an integrated system that will lead to enhanced performance and new market areas for penetrometers. The integrated technology combines steerability, vibratory pushing, and real time tracking of penetrometers into a full-scale field deployable system.

In the area of steerability, the results of integrated design led to a steering tip integrated with POLO, steerable and locking rod joints and a steering torque mechanism. In the areas of vibratory pushing and real time tracking, the design work led to integration of the POLO system and an anchoring system with the META-DRILL.

Specific results of each task were as follows:

Task 2.1 Systems Analysis

All the sub-systems were analyzed for integration into a full-scale system. Operational envelopes for all the sub-systems were defined and were shown in graphical format. The simulation model developed for these definitions can be used for design purposes in varying soil conditions. Also, additional simulations can be run for specific sites before full-scale testing, in order to obtain a general knowledge about the expected performance of the system.

Task 2.2 Steerable System Component Integration

Steerable system components were designed for integration into a full-scale system. The components included the steering tip, steerable rod joints and their locking mechanism, and a steering torque mechanism.

Task 2.3 Vibratory Penetrometer System (VPS) Integration

META-DRILL was used as the main platform for the VPS. The steerable systems of task 2.2 along with the POLO system and an anchoring mechanism were designed for integration with the META-DRILL. The POLO system integration included Quick-Connects for transmission of POLO strain gage signals to the surface computer. The devised anchoring system includes a pair of screw anchors on each side of the META-DRILL rig. Each pair of screw anchors is tied together through an anchor block.

7.0 REFERENCES

[1] Amini, A. and J. Shenhar, "A Steerable/Distance Enhanced Penetrometer Delivery System" Phase I Final Report, UTD, Inc., Newington, Virginia, 1995.

[2] Fisk, A., D. Freed, and S. Gauthier, "Development of a Steerable Pneumatic Piercing Tool" Proceedings of North American NO-DIG '95, May, 1995.

APPENDIX A

SIMULATION OF THE PENETRATION PROCESS

A.1 SIMULATION MODEL

In Phase I a simulation model was developed based on the "simple beam theory" to calculate the trajectory of a steerable penetrometer. In Phase II the simulation model was enhanced to compute the related force-couple triads along the penetrometer string of rods. A cantilever beam has been selected as the fundamental element of the trajectory. Using the following symbol definitions, the deflection and rotation of the beam's free end are given, respectively:

tip-point force	Q_p (lb)
passive distributed skin force per unit length [2,3]	q_p (lb/in)
at-rest distributed skin force per unit length [2,3]	q_0 (lb/in)
beam element length	l_i (in)
rod material modulus of elasticity	E (psi)
rod cross-sectional moment of inertia	I (in^4)
resultant tip force orientation angle	θ_r (^{0})

$$y_i = \frac{Q_p \sin\theta_r l_i^3}{3EI} + \frac{(q_p - q_0) l_i^4}{8EI} \operatorname{sgn}\theta_r \qquad (A.1)$$

$$\theta_i = \frac{Q_p \sin\theta_r l_i^2}{2EI} + \frac{(q_p - q_0) l_i^3}{6EI} \operatorname{sgn}\theta_r \qquad (A.2)$$

where "sgn" represents the standard sign function defined as

$$\begin{aligned} \theta_r > 0 \quad & \operatorname{sgn}\theta_r = 1 \\ \theta_r = 0 \quad & \operatorname{sgn}\theta_r = 0 \\ \theta_r < 0 \quad & \operatorname{sgn}\theta_r = -1 \end{aligned} \qquad (A.3)$$

The modeled trajectory is an evolution of sequential additions of one beam to another in a tail-to-head fashion. Elements of the penetrometer rod simulation model with their applied and internal force systems, are displayed in Figure A.1.

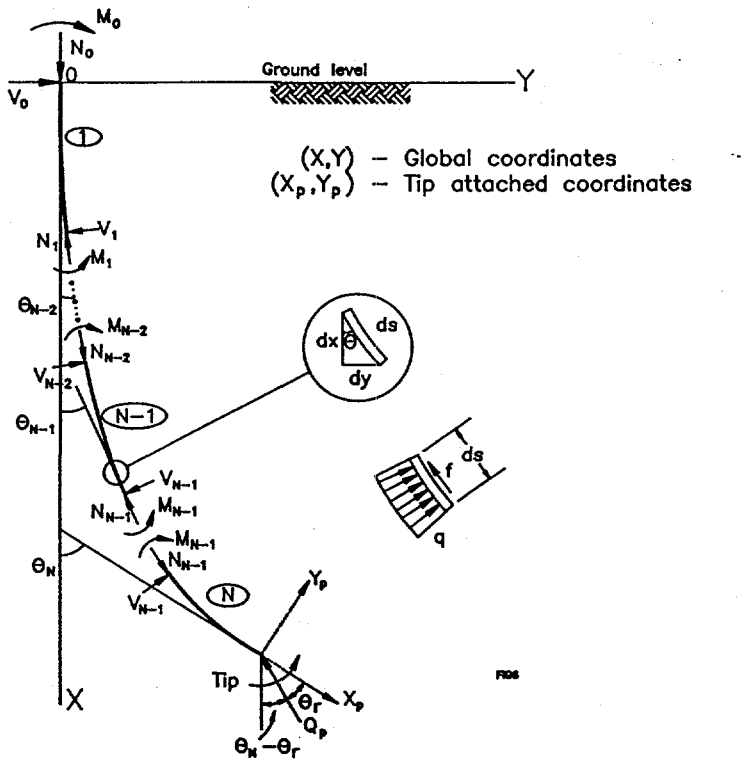

Figure A.1. Penetrometer rod simulation model

The model is comprised of N beam elements. The triad V_i, N_i, and M_i represent shear force, normal force, and a couple at joint i, respectively. i=0 symbolizes the first joint, at the connection to the insertion apparatus, while i=N, is the tip point, representing the leading edge of the penetrometer rod. X,Y, and Θ represent the variable coordinates and rotation along the rod trajectory in a fixed coordinate set X,Y. X_p,Y_p are tip-point attached set of coordinates, q is the resultant skin force per unit length (q_p-q_0), and f represents the skin friction force per unit length.

The static equilibrium conditions for element i, bounded by its joints i-1 and i, may be expressed by the following set of equations:

$$\sum F_Y = 0; \quad \int_{(i-1)}^{(i)} q(s)\cos\Theta ds - \int_{(i-1)}^{(i)} f(s)\sin\Theta ds - V_i\cos\Theta_i - N_i\sin\Theta_i + V_{i-1}\cos\Theta_{i-1} + N_{i-1}\sin\Theta_{i-1} = 0 \tag{A.4}$$

$$\sum F_X = 0; \quad -\int_{(i-1)}^{(i)} q(s)\sin\Theta ds - \int_{(i-1)}^{(i)} f(s)\cos\Theta ds + V_i\sin\Theta_i - N_i\cos\Theta_i - V_{i-1}\sin\Theta_{i-1} + N_{i-1}\cos\Theta_{i-1} = 0 \tag{A.5}$$

$$\begin{aligned}\sum M_{(i-1)} = 0; \quad & \int_{(i-1)}^{(i)} q(s)\,[\cos\Theta\,(X-X_{i-1}) + \sin\Theta\,(Y-Y_{i-1}]ds \\ & + \int_{(i-1)}^{(i)} f(s)\,[\cos\Theta\,(Y-Y_{i-1}) - \sin\Theta\,(X-X_{i-1}]ds \\ & + (-V_i\sin\Theta_i + N_i\cos\Theta_i)(Y_i - Y_{i-1}) \\ & + (-V_i\cos\Theta_i - N_i\sin\Theta_i)(X_i - X_{i-1}) + M_i - M_{i-1} = 0\end{aligned} \tag{A.6}$$

Given the tip force Q_p and its orientation angle Θ_r with respect to the rod longitudinal axis, the tip shear force, normal (axial) force, and couple may be written as:

$$\begin{aligned} V_N &= -Q_p \sin\Theta_r \\ N_N &= Q_p \cos\Theta_r \\ M_N &= 0 \end{aligned} \qquad \text{(A.7)}$$

Expressions (A.7) may serve as initial values for the set of recursive equations (A.4) to (A.6), generating a procedure to determine the triads V_i, N_i, and M_i at all of the remaining joints, i = 0,1,2,...,N-1. In practice, N_0, the normal force at the insertion point, may be measured by a load cell. This measurement may be used to validate, in part, the recursive computations.

A.2 SIMULATION MODEL APPLICATION

Employing the simulation model, penetrometer rod trajectory as well as the related force-couple triads at the joints, were computed for given soil and rod material parameters.

Soil parameters - sandy clay:

density	$\gamma = 120$ lb/ft^3
angle of internal friction	$\phi = 20^0$
surface static friction angle	$\delta = {}^2/_3\ \phi$
soil cohesion	$c = 17$ psi
bearing capacity factor	$Nc = 30$
bearing capacity factor	$Nq = 12$
adhesion factor	$\alpha = 0.42$
null earth pressure coefficient [2,3]	$K_o = 1\text{-}\sin\phi$
passive earth pressure coefficient [2,3]	$K_p = \tan^2(45+{}^{\phi}/_2)$

Penetrometer rod parameters:

rod outer diameter	$D = 1.75$ in
rod inner diameter	$d = 1.00$ in
male thread base diameter	$D_0 = 1.54$ in
total length of pile	$L = 7$ ft
rod modulus of elasticity	$E = 28*10^6$ psi

The following three figures display the simulation output. Figure A.2 provides a comparison between the rod simulated trajectory and the field test data set obtained in Phase I. The correlation between the two data sets enhances the confidence in the simulation model and therefore, the model may be used as a predictive tool for future real-time field work.

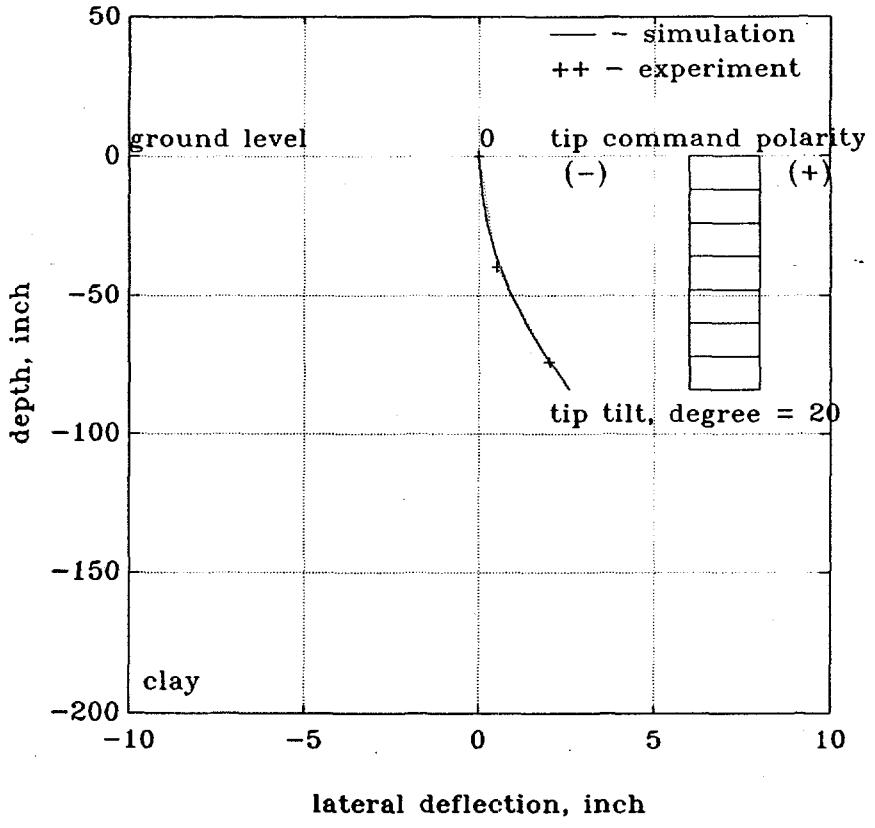

Figure A.2. Penetrometer rod trajectory - comparison between simulation results and test data.

The simulated normal (axial) force distribution along the rod is displayed in Figure A.3. The close-to-linear characteristics of the force curve is mainly due to the relative short rod and the small lateral deflection. Regardless of whether the rod is in its "push" mode with all external forces applied, or in its "idle" mode between two shoves, the bending couple along the rod may be determined directly from the rod curvature.

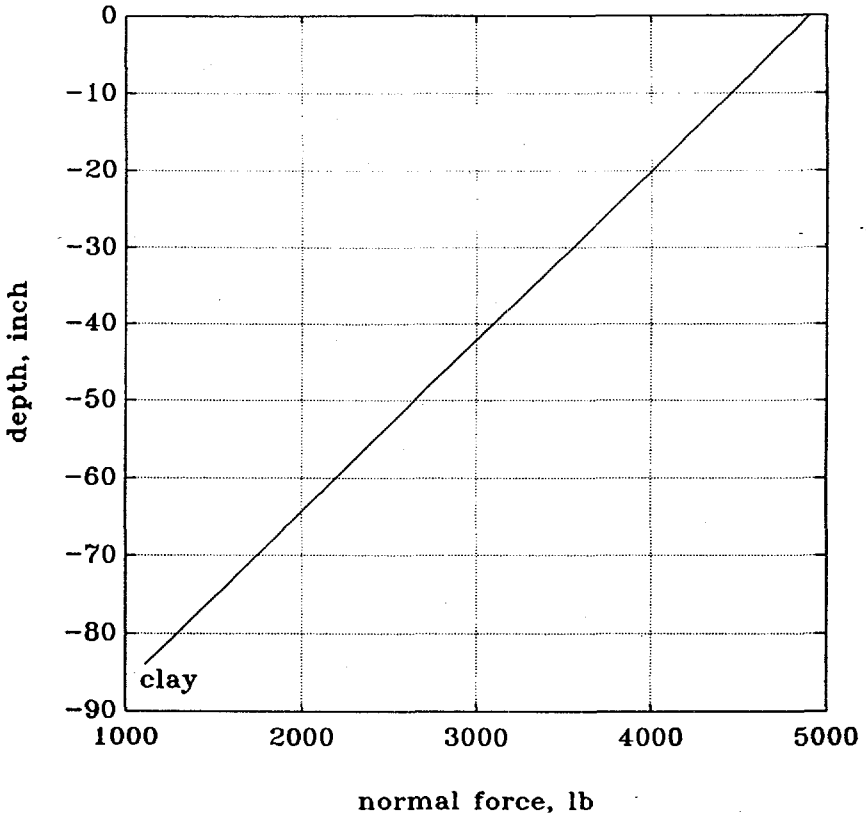

Figure A.3. Normal force distribution along the rod - simulation results.

Figure A.4 depicts the simulated characteristics of the local radius of curvature. Due to the relative short rod, the overall curvature appears to be close to circular and therefore, the bending couple does not vary significantly along this rod segment. The computed normal force and bending couple along the penetrometer rod are used to partially establish an operational envelope for the entire rod system.

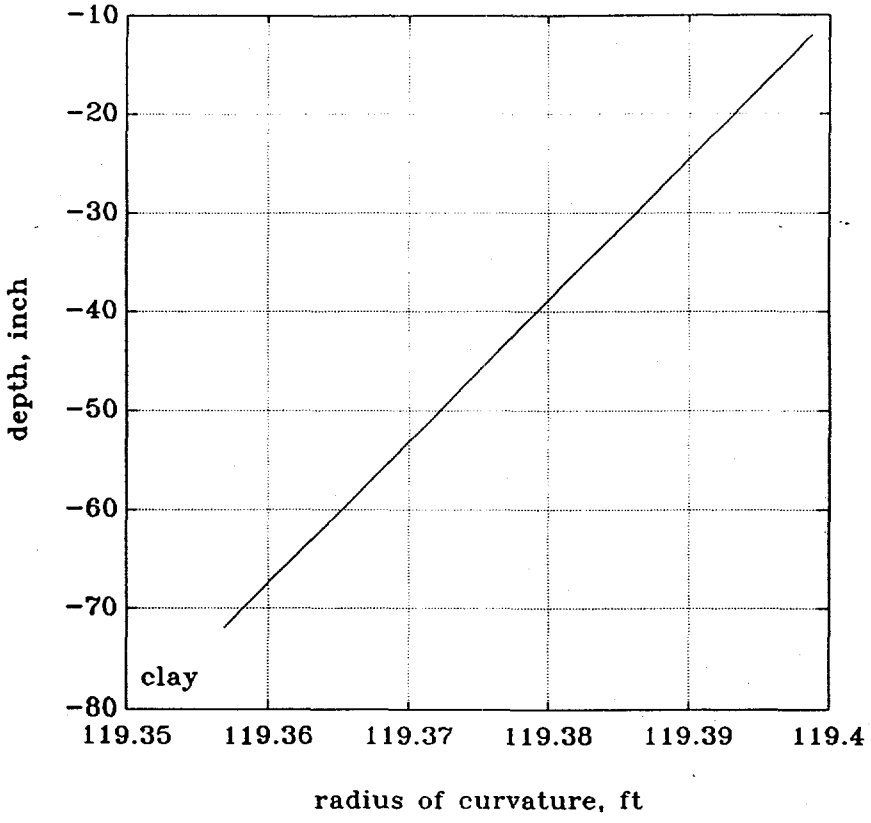

Figure A.4. Local radius of curvature simulation results.